Talbot lithography: Self-imaging of complex structures

A. Isoyan,[a] F. Jiang, Y. C. Cheng, and F. Cerrina[b]
Center for NanoTechnology, University of Wisconsin-Madison, Wisconsin 53706

P. Wachulak, L. Urbanski, J. Rocca, C. Menoni, and M. Marconi
NSF ERC for Extreme Ultraviolet Science and Technology, Department of Electrical and Computer Engineering, Colorado State University—Fort Collins, Colorado 80523

(Received 21 July 2009; accepted 5 October 2009; published 3 December 2009)

The authors present a self-imaging lithographic technique, capable of patterning large area periodic structures of arbitrary content with nanoscale resolution. They start from the original concept of Talbot imaging of binary gratings—and introduce the generalized Talbot imaging (GTI) where periodic structures of arbitrary shape and content form high-definition self-images. This effect can be used to create the complex, periodic patterns needed in the many lithographic fabrication steps of modern semiconductor devices. Since the process is diffraction limited, the achievable resolution depends only on the wavelength, mask patterning, and degree of coherence of the source. Their approach removes all the complex extreme ultraviolet (EUV) reflective masks and optics, replacing them with nanopatterned transmission masks and makes the whole process simple and cost effective. They have successfully verified the GTI concept using first a He–Ne laser, and then demonstrated its potential as a nanolithography method using a compact table-top soft x-ray (EUV) 46.9 nm laser source. These sources provide the high degree of coherence needed by diffraction-based imaging and are extendable to shorter wavelengths. They have recorded EUV GTI images up to the sixth Talbot plane, with consistent high quality good results, clearly demonstrating the ability of the GTI method to record high-resolution patterns at large distances. © *2009 American Vacuum Society.* [DOI: 10.1116/1.3258144]

I. INTRODUCTION

The semiconductor industry continues in its relentless pursuit of miniaturization, so that every 3 years or so, the dimensions of the features on an integrated circuit are halved, yielding an increase in density and functionality of electronic circuits. The economic advantages of more devices per unit area outweigh increases in fabrication costs and performance limitations, pushing the industry to seek ever-smaller patterns. As the electronics industry continues to shrink the device size in integrated circuits, optical lithography will reach its practical resolution limit. The semiconductor industry is currently considering the transition from 193 nm to extreme ultraviolet (EUV) lithography, which is based on the use of radiation of wavelength around 13 nm, a region where all materials are highly absorptive and hence only multilayer-coated reflective optics can be used to form images of the patterns to be printed. One of the main problems of EUV lithography is that EUV optical systems are complex and expensive, and today only few exposure tools are available[1] thus limiting the development of the technology.

An alternative path to the development of EUV lithography can be found in the use of diffractive optics. The interference of two coherent beams generates patterns of high-density fringes, and these fringes can be recorded in photoresist.[2] Using radiation around 13.4 nm it is possible to pattern nanostructures (see review in Ref. 3). Since it does not require complex optics while producing excellent, high-modulation images EUV lithography (EUV-IL) is been used very successfully in the development of advanced photoresists for the next generation lithographic technologies.[4] It can create one- or two-dimensional periodic patterns using various configurations, yielding periodic nanostructures with sub-50 nm resolution.[5] Higher diffraction orders provide the extension of the traditional interferometric lithography technique to produce periodic structures with a reduction factor of 4X.[6] EUV-IL by its nature is limited to periodic structures of dense lines or array of holes or triangles. Holographic projection lithography is the natural extension of this technique to generate arbitrary structures.[7,8] The development of compact high flux EUV lasers provides an opportunity to efficiently use interference and coherent imaging for patterning nanometer scale features over large areas.[9] Thus, the combination of nanopatterning techniques (mask fabrication) and coherent EUV sources (illumination) allows the creation of complex imaging patterns without complex optical systems.

In this work, we report the development of a novel high-resolution patterning approach, capable of patterning large area periodic structures of arbitrary content with nanoscale resolution. It is based on Talbot imaging (TI)—extended to the generalized Talbot imaging (GTI). The general idea of GTI is illustrated in Fig. 1: a periodic object, historically a simple linear grating, forms highly accurate real images of itself at distances that are integer multiples of a fundamental unit, the Talbot distance Z_{nT} (in our experiment Z_T=1 mm). At these locations phase shifts cancel out and the interfer-

[a]Electronic mail: isoyan@wisc.edu
[b]Electronic mail: fcerrina@wisc.edu

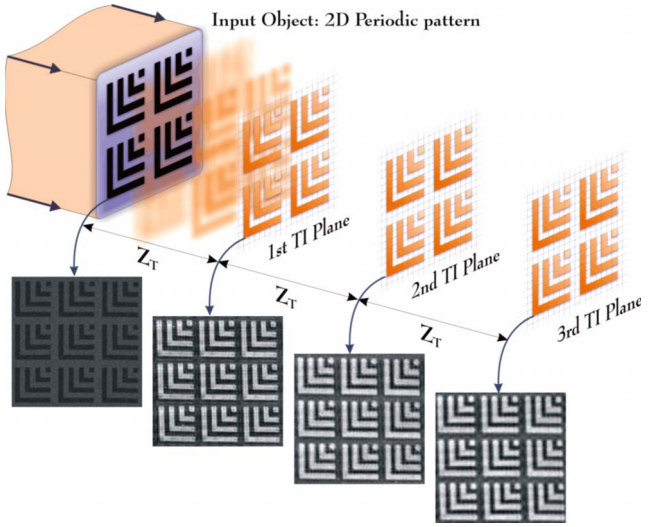

FIG. 1. (Color online) Talbot effect: First experimental results in soft x rays (EUV). The mask (first to the left) creates images at the Talbot planes [atomic force microscope (AFM) images of actual exposures]. The size of the images shown here is 14.5×14.5 μm^2, the individual lines being 500 nm and $Z_T=1000$ μm; only a small area of the mask and exposed patterns is shown for illustrative purposes. Notice the excellent quality of the images at the Talbot planes.

ence of the waves diffracted by the periodic structures recreates the image of the object—without the necessity of any optics. Clearly, GTI is an extension of the classical TI. Interestingly, this more general aspect of TI has received only very little attention in the century and a half elapsed since the original discovery by Talbot[10]—this can be attributed to the difficulty of creating high-resolution periodic patterns, a topic of little, if any interest until the advent of the semiconductor industry, and to the concomitant need for highly coherent sources. In addition, the development of excellent imaging optics did obviate the need for exploiting the properties of self-imaging objects except for the few areas where no optical system can be easily built. X-ray and EUV are two such regions of great interest for imaging and nanofabrication.

We have demonstrated that the combination of a coherent illumination source with a nanofabricated Talbot template allows for the extension of nanolithography in a relatively simple setup: the Talbot template embodies both the information to be written in the exposure field and the image formation system. An advantage of this technique is that any defect on the original mask object is averaged over the entire imaging field, and since the defect/image ratio is, in general, small, the formed image is defect free (see discussion below). The focal or working distance between mask and wafer is also very large. In its simplicity, Talbot imaging opens the door to novel application of nanolithography of periodic patterns, such as high-density memories or magnetic media, where a regular pattern is repeated over and over the area of the field. The ability to form a projected self-image of a complex periodic object has great interest in semiconductor and device fabrication—if one could extend the imaging to the nanometer region.

In this article we report the results of an initial demonstration of GTI using several coherent illumination sources. In Sec. I, we present a brief introduction into GTI theory. The mask design and fabrication flow is described in Sec. II, followed by Sec. III describing the results of GTI at 632.8 nm He–Ne laser source and EUV (soft x-ray) table-top 46.9 nm laser source.

II. GTI THEORY

While there is a sizable literature on the Talbot effect involving simple periodic gratings,[11,12] little is available for the more complex case of repeated arbitrary patterns. Let $T(x)$ be the one-dimensional transmission of the object, with $T(x)=T(x+p)$; T can be real, or complex. A simple Fourier analysis yields

$$T(x)=\sum_m C_m \exp\left\{i2\pi\frac{mx}{p}\right\}, \tag{1}$$

where C_m is the Fourier coefficient, with p the period of the pattern.

The incoming electric field $U_{\text{in}}(x,z=0)$ is first transmitted by the object, and then propagates in free space. An extensive analysis of the self-imaging properties of a simple binary grating has been discussed in Ref. 13; while higher orders m introduce and additional phase shift proportional to n^2, for the purpose of this article we limit our discussion to the case of the paraxial approximation; a more detailed analysis of the imaging properties will be published elsewhere.[14] The propagating field is calculated using Fresnel diffraction, in the simple Fresnel–Kirchhoff approximation,

$$U_{\text{Trans}}(x',z)=\frac{1}{\lambda i}\int_{-\infty}^{+\infty} U_{\text{in}}(x,z=0)T(x)\frac{e^{-ikR}}{R}dx, \tag{2}$$

where $k=2\pi/\lambda$ and $R=\sqrt{(x-x')^2+z^2}$.

Assuming the incoming electric field at normal incidence to be of unit amplitude, $U_{\text{in}}=1$, normal incident plane wave, by inserting Eq. (1) in Eq. (2) in conjunction with the standard Fresnel approximation, after Fourier transformation we obtain the electric field at a distance z as

$$U_{\text{Trans}}(x',z)\propto\sum_m C_m \exp\left(i2\pi\frac{m(x-x')}{p}\right)\exp\left(\frac{i\pi m^2\lambda z}{p^2}\right). \tag{3}$$

A self-image is observed after a certain propagation distance z_T if the expansion of the object (1) and that of the transmitted electric field (3) are identical. This may happen if and only if

$$\exp\left(\frac{i\pi m^2\lambda z}{p^2}\right)=1 \tag{4}$$

for any value of m (integer). This defines the distances z_{nT} (Ref. 15) where the paraxial propagation distances satisfies the condition

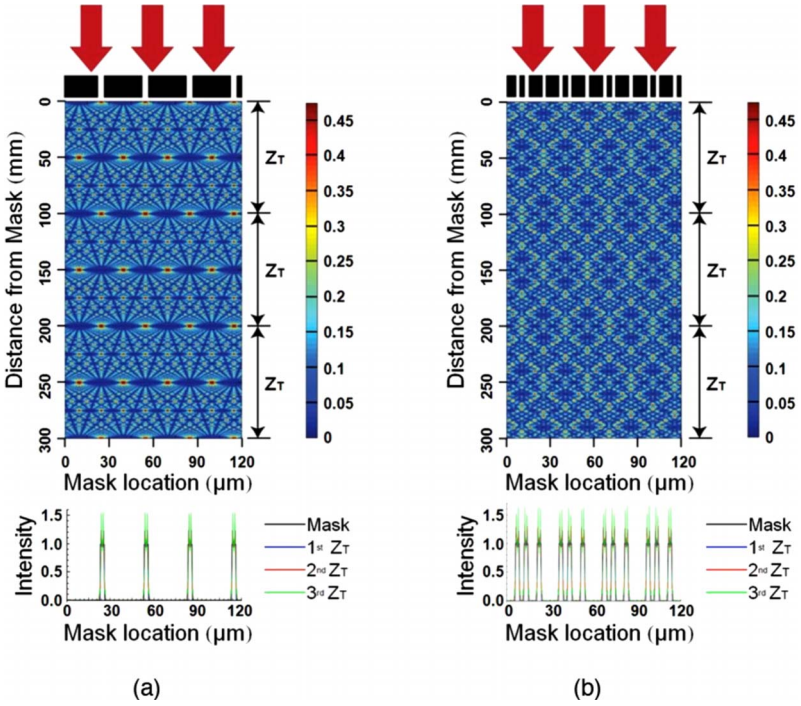

FIG. 2. (Color online) Talbot "carpet," depicting the intensity of the radiation (impinging from the top) along the propagation direction. The left panel shows the case of a simple grating, the right panel that of a more complex object. Notice the self-images at the z_{nT} locations (Talbot effect); laterally displaced self-images are observed at the half-integer positions. However, for the GTI case, no fractional pattern is observed. The figures below the carpets show the intensity profile (cut lines) at the Talbot planes; the similarity is remarkable, although difficult to visualize on the scale of the figure.

$$\frac{\pi\lambda z_{nT}}{p^2} = n2\pi \rightarrow z_{nT} = n2p^2/\lambda = nz_T, \tag{5}$$

where n is an integer and z_T is the same Talbot distance derived by Lord Rayleigh in 1881.[16] We note that in the GTI there is no connection between z_{nT} and the near-field Fresnel number, $N_F = a^2/\lambda z$, where a is the feature width, not the period.

Using a similar proof, any two-dimensional arbitrary periodical pattern will also form self-images at the propagation distance $z = z_T$, as long as the periodicity is the same in the two directions. We note that the final image is formed by the superposition of the orders coming from all the contributing unit cells, so that individual defects are averaged out and contribute very little energy to the image power spectrum.

Figure 2 shows the map of the intensity of the radiation transmitted by a periodic linear grating (the simplest type of pattern) and by a more complex periodic structure. In the first case, we can see clearly how the image is reconstructed at the different Talbot planes located at distances z_T. A simple geometrical optics analysis further shows that these Talbot planes correspond to the distance where all the diffraction orders overlap, thus reconstructing the original object, or mask. Most important, this overlap repeats periodically so there are a large number of Talbot images (infinite for a perfectly coherent illumination and an infinitely wide object, as foreseen by Talbot). There is a rich set of diffraction phenomena that can be observed in a Talbot system.[17] As the value of p/λ decreases, other effects (e.g., nonparaxial propagation, polarization) must be included explicitly;[13] as discussed below, in the experiment section we have observed excellent imaging up to the sixth Talbot plane.

III. MASK DESIGN AND FABRICATION

The analysis of the case of a simple linear grating system in TI assumes that the grating is infinite. In practice, we must consider the effect of the finite size of the mask due to the fabrication and other experimental limitations. To start with, the desired pattern to be printed on the wafer is the mask pattern. The question that arises are: (1) what is the optimal size of the mask that should be designed for GTI, and (2) what is the resolution that is attainable with such an imaging system in realistic conditions of finite partial coherence. A simple argument provides a guide to the answer. Let $2W$ be the lateral size of the Talbot mask template. The angle α subtended by the template at the sample position, i.e., at a distance z_T, is then given by

$$\sin(\alpha) = W/\sqrt{W^2 + z_T^2} = 1/\sqrt{1 + (z_T/W)^2} = \mathrm{NA}. \tag{6}$$

This is the numerical aperture of an equivalent image-forming optical system, converging with aperture NA $= \sin(\alpha)$ to the sample. In this case it is a "virtual" NA, since no optics exist to limit the angle. Alternatively, we can note that the size of the Talbot template determines how many diffraction orders can illuminate the center of the image, and thus the resolution; this latter point of view is essentially identical to the former.

If λ is the wavelength of illumination, then the diffraction limit is given by

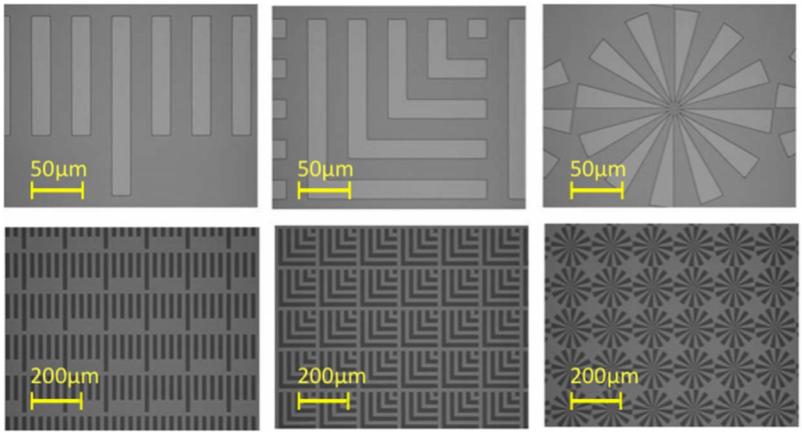

FIG. 3. (Color online) Optical microscope images of the GTI mask.

$$\Delta = \lambda/2NA = (\lambda/2)\sqrt{(1 + (z_T/W)^2)}, \tag{7}$$

i.e., the resolving power is proportional to the size of the template, and inversely proportional to the Talbot plane distance (the resolution Δ is essentially $p/2$, where $p=1/f_{\text{cutoff}}$ of coherent imaging). Further simplifying the relation, we obtain

$$\Delta_n = (\lambda/2)\sqrt{1 + \left(\frac{2np^2}{\lambda W}\right)^2}, \tag{8}$$

showing how the resolution improves for smaller periods, larger widths of the object, and smaller Talbot distances. In other hand the total number of unit cells in the mask should be equal $M=2W/p$. As follows from Eq. (8) the number of cells in the mask for n Talbot imaging plane can be written as

$$M = \frac{4np}{\sqrt{((2\Delta_n)^2 - \lambda^2)}}. \tag{9}$$

For the case of radiation around 13.4 nm, with an object of period $p=1$ μm, target resolution $\Delta_n=10$ nm, when using $n=1$, we obtain $M=270$ with a NA=0.67. Also we can clearly see that the resolution limit of the GTI equals $\lambda/2$.

As in all imaging systems, the depth of focus depends on the resolution and on the numerical aperture of the system. For a diffraction limited system, we have that

$$\text{DOF} = \frac{\lambda}{(\text{NA})^2} = \lambda\left[1 + \left(\frac{2np^2}{\lambda W}\right)^2\right], \tag{10}$$

where the DOF refers to the length of the region of good imaging.[18] As a demonstration of self-imaging lithography, we decided to print standard lithographic resolution test patterns. The design of the self-imaging template, or mask, is relatively simple, with identical periods in the x and y directions. For a given wavelength and image position (also called "focal distance," as explained below) we compute the period of the two-dimensional object that will yield the correct z_T. The actual fabrication process of EUV mask is based on one of the standard processes developed at CNTech for creating EUV-IL optics. For the 632.8 nm wavelength He–Ne laser source we fabricated the mask on a rectangular quartz substrate coated with 200 nm thick Cr. Three different patterns were fabricated. The optical microscope images of the mask are shown in Fig. 3. The mask total width is 23 mm and it contains 123 unit cells repeated in x and y directions, which corresponds to 3.6 μm target resolution. The designed Z_T Talbot distance is 10.24 cm, unit cell period is 180 μm.

For the soft x-ray (EUV) table-top laser system, the mask was fabricated on a ultrathin membrane to yield a high transmissivity at 46.9 nm. We use 25 nm of SiNH silicon-rich nitride as the carrier, with a transmission $T \cong 13.5\%$ at 46.9 nm wavelength.[19] The Talbot template was patterned using standard electron-beam lithography in a 65 nm thick hydrogen silsesquioxane photoresist. This film efficiently absorbs the radiation at 46.9 nm, with a transmission of approximately 3%.[19] The field size of the mask is approximately 600×600 μm at a distance of 1 mm for the first Talbot plane (Fig. 4). The period of the patterns in the mask was 4.845 μm, and the smallest features were 140 nm. We note that in order to have a point resolution of 100 nm at the soft x-ray (EUV) wavelength of 46.9 nm, the Talbot mask

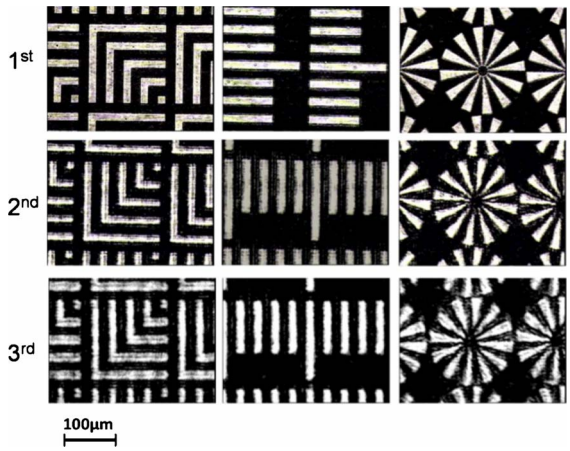

FIG. 4. (Color online) Digital charge-coupled device (CCD) camera recorded images of Talbot imaging at first (10.24 cm), second (20.48 cm), and third (30.72 cm) Talbot planes using He–Ne laser light. Notice the ringing due to the highly coherent imaging conditions.

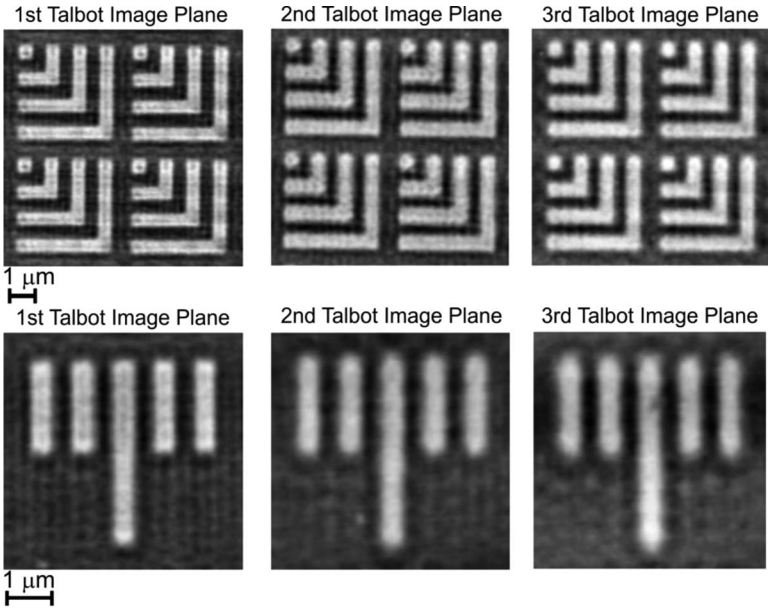

FIG. 5. AFM images of 500 nm test patterns recorded at several Talbot planes in 50 nm thick PMMA.

must have a numerical aperture of at least ≈0.28; thus, the cell of the mask should be repeated in each direction at least 124 times. We note that the use of shorter wavelengths will allow the use of much thicker mask carriers, $t_{\text{membrane}} \geqslant 100-200$ nm, thus providing much more stable support.

IV. EXPERIMENTAL RESULTS

At first, we used a simple GTI demonstration using He–Ne 632.8 nm wavelength coherent illumination. The experimental setup of the GTI is very simple and does not include any complicated alignments and adjustments. The GTI fabricated mask has been designed to have 180 μm period, hence the first Talbot distance is 10.24 cm. The field size of the mask is 2.2×2.2 cm^2, yielding 0.11 numerical aperture at the first Talbot distance, which has the ability to resolve 3.5 μm resolution. These exposure results are shown in Fig. 5. In addition, we show in Fig. 6 the atomic force microscope (AFM) image of a set of 140 nm test patterns rotated at 45° relative to the periodic directions, to show explicitly the ability to print arbitrary features.

For the demonstration of GTI at 46.9 nm wavelength illumination we have used a highly coherent table top soft x-ray (EUV) laser developed at Colorado State University. The compact Ne-like Ar capillary discharge laser used in this experiment is configured to produce pulses with energy of approximately 0.1 mJ of 1.2 ns full width at half maximum (FWHM) duration. It can be operated at repetition rates of several hertz producing average power levels in excess of 1 mW with high degree of spatial and temporal coherence. The laser operates using the 46.9 nm $3s1P1-3p1S0$ transition of Ar^{+8} ion. An alumina capillary of 3.2 mm in diameter and 27 cm in length filled with Ar is excited with a current pulse approximately 22 kA, a 10%–90% rise time of approximately 55 ns, and a first half-cycle duration of approximately 135 ns.[20,21] The relative band width of the soft x-ray (EUV) laser is approximately $\Delta\lambda/\lambda=10^{-4}$, yielding a coherence length of approximately 470 μm. The spatial coherence length of the beam is calculated to be 740 μm at the distance where the exposure took place. We note that the spatial coherence increases when the capillary length is increased, reaching an almost fully spatial coherent beam for capillaries 36 cm in length.[22]

The capillary discharge laser equipped with a 27 cm long capillary illuminates the Talbot mask placed 219.5 cm away from the laser. That assures that the beam coherence radius is larger than the size of the single Talbot mask, i.e., ≈650 $\times$650 μm^2. A polymethyl-metacrylate (PMMA) coated sample was placed in the vicinity of the calculated working

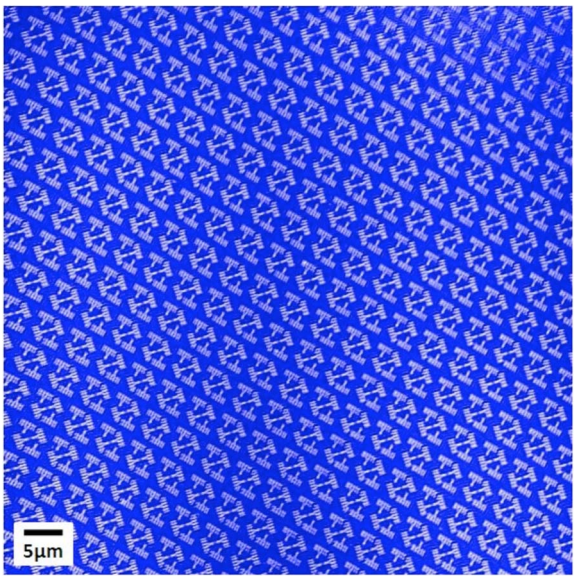

FIG. 6. (Color online) AFM images of 140 nm test patterns rotated by 45° recorded at the first EUV Talbot plane in 50 nm thick PMMA.

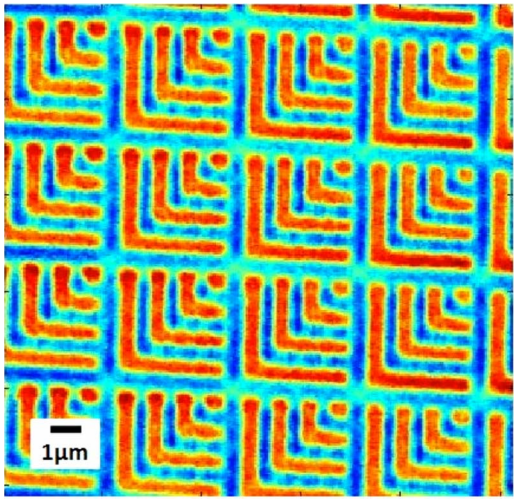

FIG. 7. (Color online) AFM scan of Talbot imaging on the sixth plane. The sixth Talbot distance is ≈6 mm, and the pattern is still imaged faithfully.

distance of the first Talbot plane, equal to 1 mm. The self-image of the Talbot mask was generated at this distance and recorded by the photoresist.

Typical patterns obtained with an AFM are shown in Fig. 5. The consistency between the images is remarkable and clearly demonstrates the excellent imaging fidelity of the process. We note that for the sake of verification, the samples were also imaged in an SEM (not shown here), yielding similar results, but because of the very thin resist used ($t \leqslant 50$ nm) the scanning electron microscope (SEM) image quality is poor. Finally, we show that images were recorded up to the sixth Talbot plane, with good results. We want to note that the sixth talbot plane is not the limit of the GTI mask, being rather the experimental limit since the sample holder stage had only 7 mm working distance. This clearly shows the ability of the method to record high-resolution patterns at large distances.

V. CONCLUSION

The power of Talbot imaging is evident in the impressive sequence of images shown in Fig. 7. We note that we have recorded excellent images up to the sixth Talbot plane. The technique opens very interesting imaging possibilities, since it does not rely on complex optical systems but rather on the fundamental principles of diffraction and free-space propagation. GTI must not be confused with proximity imaging, as the latter works with the sample in close proximity of the object, i.e., at Fresnel numbers less than 1.

Generalized Talbot imaging is ideally suited for highly coherent illumination sources, as demonstrated in our experiment. Its realization relies entirely on the development of short wavelength (high photon energy) sources of sufficient coherence in the soft x-ray (EUV) spectral region. It can be expected that the continuing development of table top laser-excited soft x-ray (EUV) lasers capable to emit in the wavelength region below 20 nm (Refs. 23 and 24) can improve the spatial resolution of table top nanolithography even further, to features only limited by the photoresist resolution and our ability to pattern the original mask. These developments will enable the demonstration of a practical nanopatterning tool for the quick fabrication of large arrays of periodic features that so far were restricted to the use of large synchrotron facilities and opens the possibility of a completely new fabrication approach even for large scale nanolithography with dimensions of less than 10 nm over areas as large as several mm^2. Finally, there is no reason to limit GTI to the canonical EUV wavelength of 13.4 nm: the same method can be applied to shorter wavelengths when these will become available, thus extending the imaging ability of the process. In summary, the Talbot imaging is limited by three factors: Our ability to pattern the template, the wavelength of the illuminating source, and its degree of coherence.

ACKNOWLEDGMENTS

This work was supported in part by the NSF Engineering Research Center for Extreme Ultraviolet Science and Technology under NSF Award No. EEC-0310717 and by the NSF UW Nanoscale Science and Engineering Center (No. DMR-0425880). F.J. was supported by the SRC Contract No. 2005-OC-985-985.007. This work used the facilities and staff at the UW Synchrotron Radiation Center (NSF Grant No. DMR-0084402), the UW Center for Nanotechnology (CNTech), and the Wisconsin Center for Applied Microelectronics (WCAM). Electron Beam Lithography was performed at the Center for Nanomaterials (CNM) at Argonne National Laboratory.

[1] B. J. Lin, J. Microlithogr., Microfabr., Microsyst. **5**, 33005 (2006), and the references therein.
[2] T. A. Savas, M. L. Schattenburg, J. M. Carter, and H. I. Smith, J. Vac. Sci. Technol. B **14**, 4167 (1996).
[3] F. Cerrina, J. Micro/Nanolith. MEMS MOEMS **8**, 021201 (2009).
[4] R. Gronheid and M. J. Leeson, J. Micro/Nanolith. MEMS MOEMS **8**(2), 021205 (2009).
[5] V. Auzelyte *et al.*, J. Micro/Nanolith. MEMS MOEMS **8**, 021204 (2009).
[6] A. Isoyan, A. Wüest, J. Wallace, F. Jiang, and F. Cerrina, Opt. Express **16**, 9106 (2008).
[7] Y.-C. Cheng, A. Isoyan, J. Wallace, M. Khan, and F. Cerrina, Appl. Phys. Lett. **90**, 023116 (2007).
[8] F. Jiang, Y.-C. Cheng, A. Isoyan, and F. Cerrina, J. Micro/Nanolith. MEMS MOEMS **8**, 021203 (2009).
[9] P. W. Wachulak *et al.*, J. Micro/Nanolith. MEMS MOEMS **8**, 021206 (2009).
[10] W. H. F. Talbot, Philos. Mag. **9**, 403 (1836).
[11] A. W. Lohmann, H. Knuppertz, and J. Jahns, J. Opt. Soc. Am. A **22**, 1500 (2005).
[12] J. F. Clauser and S. Li, Phys. Rev. A **49**, R2213 (1994).
[13] E. Noponen and J. Turunen, Opt. Commun. **98**, 132 (1993).
[14] F. Jiang and F. Cerrina, (unpublished).
[15] J. W. Goodman, *Introduction to Fourier Optics*, 3rd ed. (Roberts & Company, Engelwood, CO, 2005), pp. 88–91.
[16] L. Rayleigh, Philos. Mag. **11**, 196 (1881).
[17] M. Berry, I. Marzoli, and W. Schleich, Phys. World **14**, 39 (2001).
[18] M. Born and E. Wolf, *Principles of Optics*, 7th ed. (Cambridge University Press, Cambridge, 1999), pp. 489–492.
[19] Center for X-Ray Optics, http://www-cxro.lbl.gov/.
[20] C. D. Macchietto, B. R. Benware, and J. J. Rocca, Opt. Lett. **24**, 1115 (1999).

[21]B. R. Benware, C. D. Macchietto, C. H. Moreno, and J. J. Rocca, Phys. Rev. Lett. **81**, 5804 (1998).
[22]Y. Liu, M. Seminario, F. G. Tomasel, C. Chang, J. J. Rocca, and D. T. Attwood, Phys. Rev. A **6303**, 033802 (2001).
[23]Y. Wang, M. A. Larotonda, B. M. Luther, D. Alessi, M. Berrill, V. N. Shlyaptsev, and J. J. Rocca, Phys. Rev. A **72**, 053807 (2005).
[24]Y. Wang, E. Granados, F. Pedaci, D. Alessi, B. Luther, M. Berrill, and J. J. Rocca, Nat. Photonics **2**, 94 (2008).